ACS Catalysis

Research Article

pubs.acs.org/acscatalysis

Preparation and Characterization of Pt−Ru Bimetallic Catalysts Synthesized by Electroless Deposition Methods

Weijian Diao, John Meynard M. Tengco, John R. Regalbuto, and John R. Monnier*

Department of Chemical Engineering, Swearingen Engineering Center, University of South Carolina, 301 Main Street, Columbia, South Carolina 29208 United States

ABSTRACT: Two series of Pt@Ru/C and Ru@Pt/C bimetallic catalysts have been prepared by an electroless deposition (ED) method. For Pt@Ru/C compositions, a new ED bath was developed using $Ru(NH_3)_6Cl_3$ as the Ru precursor and HCOOH as the reducing agent. For Ru@Pt/C preparations, a standard bath using H_2PtCl_6 and DMAB as the Pt precursor and reducing agent, respectively, was employed. The Pt@Ru/C and Ru@Pt/C bimetallic catalysts have been characterized by temperature-programmed reduction (TPR), selective chemisorption, X-ray photoelectron spectroscopy (XPS), and scanning transmission electron microscopy (STEM) with X-ray energy dispersive spectroscopy (XEDS). TPR and selective chemisorption (H_2 titration of oxygen-precovered surfaces) experiments have confirmed the existence of strong surface interactions between Pt and Ru, as evidenced by hydrogen spillover of Pt to Ru (Pt-assisted reduction of oxygen precovered Ru). XPS analyses also showed e^- transfer from Pt to Ru on the bimetallic surface, again indicating strong surface interactions between Pt and Ru. Finally, the STEM images and XEDS elemental maps provided strong visual evidence of targeted deposition of the secondary metal on the primary metal. The elemental maps confirmed that individual nanoparticles of both Pt@Ru/C and Ru@Pt/C catalysts prepared by ED were bimetallic, with excellent association between the primary and the secondary metals.

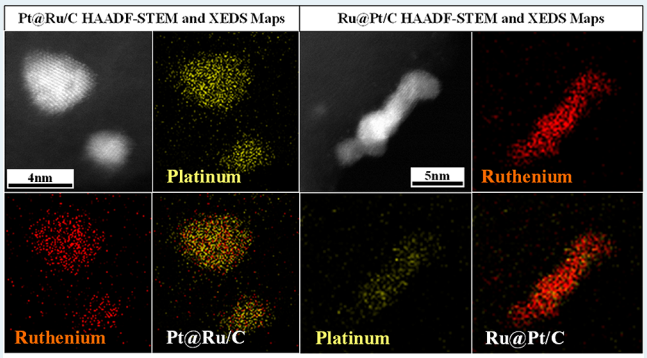

KEYWORDS: *platinum, ruthenium, electroless deposition, bimetallic catalyst, strong metal−metal interaction*

1. INTRODUCTION

The platinum−ruthenium (Pt−Ru) bimetallic system has been extensively studied since the early 1900s. Synergistic effects have been observed for a variety of reactions, primarily skeletal isomerization reactions (hydrogenolysis of C−C bonds) for catalytic reforming of alkanes to increase octane values by conversion into aromatics, cycloalkanes, and branched acyclic alkanes.[1−3] Pt−Ru catalysts have also been used for the selective hydrogenation of multifunctional olefins for the production of higher value chemicals;[4] exemplary reactions include selective hydrogenation of cinnamaldehyde,[5,6] citral,[7] *ortho*-chloronitrobenzene,[8,9] glycerol[10] and α,β-unsaturated aldehydes.[11,12] With the combination of high activity for hydrogenation of C═O bonds from Ru and facile hydrogenation ability of C═C bonds from Pt, specific Pt−Ru catalysts have shown high activity for hydrogenation of a of variety chemicals and selective hydrogenation of specific functional groups of multifunctional olefins.

More recently, Pt−Ru catalysts have been used for fuel cell applications in which alcohols are used as H_2 sources at the anode of PEM fuel cells. Specifically, it has been shown that anodic Pt−Ru catalysts provide optimal performance for direct methanol fuel cells (DMFC) relative to Pt monometallic catalysts. Platinum catalysts typically lose activity due to poisoning from strongly adsorbed CO generated during methanol reforming. The presence of surface Ru minimizes the effects of CO poisoning by the direct interaction between Ru and Pt surface sites. Electrochemical studies have suggested that the existence of the Ru−OH species (from the H_2O vapor cofeed) helps remove CO adsorbed on adjacent Pt surface sites.[13] The reaction scheme is shown in eqs 1 and 2 below.

$$Ru + H_2O \rightarrow Ru\text{-}OH + H^+ + e^- \quad (1)$$

$$Ru\text{-}OH + Pt{-}CO \rightarrow Ru + Pt + CO_2 + H^+ + e^- \quad (2)$$

This interaction can occur only when the two metallic components form bimetallic surface compositions instead of separate particles or ensembles of separate metal atoms on the catalyst surface. Several research groups[14−17] have reported that bimetallic Pt−Ru catalysts with a 1:1 bulk molar ratio give the best performance. It is intuitive that the bifunctional mechanism described above requires the Pt and Ru sites to be in contiguous positions to facilitate CO removal. However, in most cases, the Pt−Ru catalysts have been prepared by bulk methods (coimpregnation, successive impregnation, galvanostatic pulse electrodeposition)[18−21] that do not necessarily form

Received: May 14, 2015
Revised: July 23, 2015
Published: July 23, 2015

DOI: 10.1021/acscatal.5b01011
ACS Catal. 2015, 5, 5123−5134

surface compositions that are consistent with overall composition because conventional preparation methods have poor control of the surface composition; coimpregnation and successive impregnation typically result in both monometallic and bimetallic particles (of variable composition), which make it difficult to determine the position of the two metallic components.

Thus, preparative methods that form bimetallic catalysts with bimetallic surfaces of known composition should be critical to improving catalyst performance. We use the method of electroless deposition (ED) to deposit a secondary metal salt onto a pre-existing metal site that has been activated by a suitable reducing agent.[22−28] The process may include both catalytic deposition of the metal salt in solution onto the pre-existing supported metal and autocatalytic deposition of the metal salt onto the just reduced, deposited metal. In principle, however, the ED process forms only bimetallic particles without formation of isolated secondary metal particles on the catalyst support. With the kinetic control of electroless deposition, the final composition of a particular bimetallic catalyst can be controlled to give rather precise combinations of the two metallic components.

Unlike conventional bimetallic catalyst preparation methods (coimpregnation and successive impregnation), which result in both monometallic and bimetallic particles with varying composition, the electroless deposition (ED) method offers the ability to synthesize true bimetallic catalysts with bimetallic surfaces. By controlling the base catalyst, secondary metal ion source, reducing agent, bath temperature, and pH, our group has successfully synthesized multiple bimetallic catalyst systems, such as Cu−Pd,[22] Ag−Pt,[23] Pd−Co,[24] Au−Pd,[25] and Ag−Pd.[26]

In this paper, two series of Ru@Pt/C (Pt deposited on Ru surfaces) and Pt@Ru/C (Ru deposited on Pt surfaces) catalysts have been synthesized. The focus of this manuscript is limited to the preparation and characterization of these compositions. Characterization data from temperature-programmed reduction (TPR), selective chemisorption, X-ray photoelectron spectroscopy (XPS), and scanning transmission electron microscopy (STEM) are presented to confirm formation of Pt−Ru bimetallic surfaces with strong metal−metal interactions. Results for evaluation of these catalysts for direct methanol fuel cells (DMFC) are the subject of a forthcoming paper. Future work will also include evaluation of these catalysts for paraffin reforming reactions and Fischer−Tropsch applications.

2. EXPERIMENTAL SECTION

2.1. Catalyst Preparation. For Ru deposition on Pt, ruthenium(III) hexaammine chloride ($Ru(NH_3)_6Cl_3$) supplied by Sigma-Aldrich and formic acid (HCOOH, 99% purity) supplied by Fluka analysis were used as the Ru metal salt and reducing agent, respectively. $Ru(NH_3)_6Cl_3$ and HCOOH (FA) were dissolved using DI water to form separate stock solutions. The proper volumes of $Ru(NH_3)_6Cl_3$ solution and DI water were added to a Pyrex beaker to give 100 mL of ED bath and the desired initial concentrations of $Ru(NH_3)_6^{3+}$. The bath pH was adjusted to a specific value of pH 2−4 with hydrochloric acid (HCl, 36.5−38%) supplied by BDH, and the bath temperature was maintained at values of 70−120 °C by immersion into a temperature-regulated oil bath. At temperatures >100 °C, a reflux condenser was used to maintain H_2O in the ED bath. HCOOH was next added to the bath solution to determine thermal stability (no reduction of the Ru^{3+} salt by HCOOH). Stabilities were ensured over a 120 min time interval. For ED experiments, a 20 wt % Pt/XC-72 base catalyst was added to the bath after a 30 min time interval (final bath stability check). Additional aliquots of FA were added at different time intervals during the ED experiment to ensure adequate concentrations of reducing agent. One milliliter liquid aliquots were taken from the bath periodically during the deposition for Ru analysis using atomic absorption spectroscopy (AAS) performed using a PerkinElmer AAnalyst 400 spectrometer. For every ED experiment, the pH value of the bath was maintained constant at the initial pH value using a HCl solution of pH 1 and NaOH solution at pH 11.

For Pt deposition, hexachloroplatinic acid (H_2PtCl_6) and dimethylamine borane (DMAB, 97% purity), both supplied by Sigma-Aldrich, were used as the Pt salt and reducing agent, respectively. The kinetics and energetics of Pt deposition using DMAB have been described in detail in earlier work by Beard.[24,29,30] As above, H_2PtCl_6 and DMAB were dissolved in DI water to form separate stock solutions, and proper volumes of H_2PtCl_6 solution and DI water were used to form a 100 mL ED bath with the desired Pt salt content. The bath pH was adjusted to pH 9−11 using a NaOH solution (NaOH pellets from J.T. Baker.) The ED bath temperature was maintained at specific temperatures of 50−90 °C. Before ED experiments, a solution containing DMAB was added to the $PtCl_6^{2-}$ solution to check the bath stability; stability was ensured for a minimum of 60 min. For ED experiments, the 20 wt % Ru/C base catalyst was added after 30 min. Additional DMAB was also added during ED to ensure complete deposition of $PtCl_6^{2-}$. One milliliter samples were periodically taken from the bath, and the concentrations of the unreacted $PtCl_6^{2-}$ were analyzed by atomic absorption spectroscopy (AAS). All the bimetallic catalysts prepared by an electroless deposition method were washed with sufficient amounts of water (~2 L/g catalyst) to remove inorganic residues and byproducts. The catalysts were then dried in vacuo at room temperature and stored at ambient conditions in sealed bottles.

2.2. Catalyst Characterization. The concentrations of Pt and Ru surface sites for the base Pt/XC-72 and Ru/XC-72 catalysts were determined by pulse chemisorption using H_2 titration of oxygen-precovered Pt and Ru sites. A Micromeritics Autochem II 2920 automated chemisorption analyzer with a high-sensitivity thermal conductivity detector (TCD) was used for all chemisorption measurements. Before analysis, all samples were pretreated in situ in flowing H_2 for 3 h at 300 °C and then purged with flowing Ar for 0.5 h before cooling to 40 °C in Ar. A gas flow of 10% O_2/balance He was passed over the samples for 30 min to form O-covered Pt or Ru surface species. After purging with pure Ar flow for 30 min to remove residual gas phase and weakly adsorbed O_2, pulses of 10% H_2/balance Ar were dosed at 5 min intervals until all the surface oxygen reacted with H_2 to form H_2O and Pt−H or Ru−H surface species.

Previous work has shown that surface Pt−O species was easily titrated by dosing pulses of 10% H_2/Ar at 40 °C; however, titration of O−Ru sites required higher temperatures.[31] The higher temperature required for Ru−O titration will be discussed in more depth in the Results section. In this study, H_2 was dosed at 40 °C for Pt/XC-72 and at 250 °C for Ru/XC-72. The hydrogen titration stoichiometry was assumed to be H_2/Pt = 3/2 and H_2/Ru = 5/2 according to the following equations. The assignment of O/Ru = 2/1 stoichiometry is taken from the work of Corro.[32]

DOI: 10.1021/acscatal.5b01011
ACS Catal. 2015, 5, 5123−5134

H_2 titration:

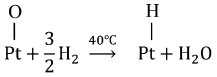

(3)

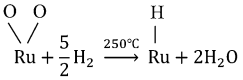

H_2 titration: (4)

Hydrogen titration experiments gave Pt and Ru dispersions of 21.5% and 5.8%, respectively, corresponding to average Pt and Ru diameters of 5.3 and 21.1 nm, respectively. The total surface sites for Pt@Ru/XC-72 and Ru@Pt/XC-72 bimetallic catalysts were also measured at both 40 and 250 °C using the same pretreatment procedure as for the monometallic catalysts.

Temperature-programmed reduction (TPR) using a CHEM-BET-3000 (Quantachrome Instruments) was used to determine optimal H_2 titration temperatures of O-precovered surfaces and the subsequent extent of Pt−Ru interactions for the bimetallic compositions. All catalysts were reduced in flowing H_2 for 3 h at 300 °C and then purged with flowing N_2 for 30 min at 300 °C before cooling to 40 °C in N_2. A gas stream of O_2 was then flowed for 30 min to form O-precovered Ru and Pt surface species. After purging with N_2 for 30 min to remove residual gas and weakly adsorbed O_2, 10% H_2/balance N_2 was passed over the sample while heating from 40 to 400 °C at 10 °C/min ramp rate. Hydrogen consumption was measured using a thermal conductivity detector (TCD).

X-ray photoelectron spectroscopy (XPS) measurements were collected using a hemispherical analyzer on a Kratos Axis Ultra DLD XPS with a monochromated Al Kα X-ray source. The monochromatic Al Kα source was operated at 15 keV and 150 W, incident at 45° with respect to the surface normal. The pass energy was fixed at 40 eV for the detailed scans. All samples were pretreated at 280 °C in H_2 for 2 h, followed by Ar flow for 2 h, and cooled to room temperature in Ar flow in a catalysis chamber attached to the UHV chamber by means of a gate valve and a linear translation arm. After pretreatment, the samples were transferred without exposing to air into the UHV chamber for XPS measurements. In this study, all catalysts were supported on highly conductive XC-72 carbon, so no charge neutralization was needed to offset surface charging. All samples were analyzed as received and after 280 °C reduction in H_2 for 2 h. The before reduction (BR) and after reduction (AR) data for C 1s, Ru $3d_{5/2}$ and Pt $4f_{7/2}$ were analyzed for all samples. All Ru $3d_{5/2}$ and Pt $4f_{7/2}$ binding energy (BE) peak positions were corrected using the C 1s binding energy value of 284.2 eV, and all peak intensities were normalized to that for the C 1s peak for quantitative comparison.

Powder X-ray diffraction (XRD) analyses of the bimetallic catalysts with highest loadings of secondary metal as well as the monometallic core nanoparticles were performed on a Rigaku Miniflex II benchtop diffractometer with a Cu Kα radiation source (λ = 1.5406 Å) operated at 30 kV and 15 mA. Powder samples were loaded onto an amorphous glass-backed, low-background holder. Scanning was done over the 2θ range of 30−75° with sampling width of 0.02° and dwell time of 2°/min. The diffractometer was fitted with a Rigaku D/tex Ultra silicon strip detector, which is capable of detecting nanoparticles in samples with metal loadings as low as 1 wt % and particles as small as 1 nm.[33]

Scanning transmission electron microscopy (STEM) was used to obtain high angle annular dark field (HAADF) images of the base catalysts and the ED prepared bimetallic catalysts using a cold field emission, probe-aberration-corrected, 200 kV electron microscope, the JEOL JEM-ARM200CF. The JEM-ARM200CF has an imaging resolution of down to below 0.078 nm and energy resolution of 0.35 eV. HAADF micrographs were acquired with either of the two detectors (JEOL and Gatan) for HAADF fitted in the JEM-ARM200CF. Microanalyses of the catalysts were done using X-ray energy dispersive spectroscopy (XEDS) to generate elemental maps of Ru and Pt. The XEDS maps were acquired through an Oxford Instruments X-Max100TLE SDD detector also fitted to the JEM-ARM200CF. The ED-prepared catalysts with the highest loading of secondary metal were selected for STEM imaging and XEDS to obtain the best possible imaging contrast and spectroscopic signal, respectively.

3. RESULTS AND DISCUSSION

3.1. Catalyst Synthesis. *3.1.1. Pt@Ru/XC-72 Preparation.* Several different Ru precursor salts were tested for development of an ED bath for Ru deposition on the Pt/XC-72 base catalyst. Most could not be used because of (1) insolubility in water (e.g., $Ru(NH_3)_6Cl_2$), (2) precipitation at basic conditions typically used for ED (e.g., K_2RuCl_5), or (3) being too stable for reduction with conventional reducing agents (e.g., $K_4Ru(CN)_6$). Consequently, $Ru(NH_3)_6Cl_3$ was selected as the preferred choice for Ru deposition. To ensure there was no strong electrostatic adsorption of $Ru(NH_3)_6^{3+}$ on the Pt/XC-72 catalyst, the pH of the reaction was maintained below the point of zero charge (PZC) of the catalyst.[34,35] In this case, the reaction was conducted at acidic conditions of less than pH 4.8, the PZC of 20 wt % Pt/XC-72. A recent study by Mustain[36] has shown that formic acid (HCOOH, FA) is an effective reducing agent under acidic solutions. Therefore, development of an ED bath using $Ru(NH_3)_6Cl_3$ as the Ru precursor and formic acid as reducing agent at acidic conditions was required for deposition of Ru on the base Pt/XC-72 catalyst. A sample weight of 0.5 g of the base 20 wt % Pt/XC-72 catalyst in a 100 mL ED bath was used for each experiment. All deposition experiments were conducted for 2 h, and the first 30 min served to test the bath stability with only the $Ru(NH_3)_6Cl_3$ precursor and formic acid present in the bath. After 30 min, the Pt/XC-72 was added to the ED bath, and additional aliquots of formic acid solution were added at 30 min time intervals to compensate for any nonselective decomposition of formic acid.

The initial set of experiments examined the effects of bath temperature on the rate and extent of Ru deposition on the Pt surface of 20 wt % Pt/XC-72. In Figure 1, the concentration of 110 ppm Ru^{3+} corresponded to one monodisperse layer coverage of Ru on the Pt surface (based on Pt chemisorption measurements, which will be discussed in Section 3.2.1). All deposition temperature values are of the oil bath and not of the aqueous solution inside the beaker/flask itself. At T > 90 °C, a reflux condenser was used to prevent evaporation of H_2O from the ED bath. From Figure 1, the first 30 min confirmed the thermal stability of the Ru^{3+} salt in the presence of FA before the addition of Pt/XC-72. In addition to the bath stability test, an earlier control experiment with only $Ru(NH_3)_6Cl_3$ and 20 wt % Pt/XC-72 in solution was also conducted at ED conditions. There was no Ru uptake at pH 3, confirming that no strong electrostatic adsorption between Ru^{3+} and the carbon support occurred. Thus, all Ru uptakes in Figure 1 must be due to electroless deposition of Ru on Pt and not adsorption on the carbon support. The deposition curves in Figure 1 also show that uptake at 70 and 90 °C ceased after ∼30 min of exposure (60 min overall time). No further Ru deposition occurred, even

DOI: 10.1021/acscatal.5b01011
ACS Catal. 2015, 5, 5123−5134

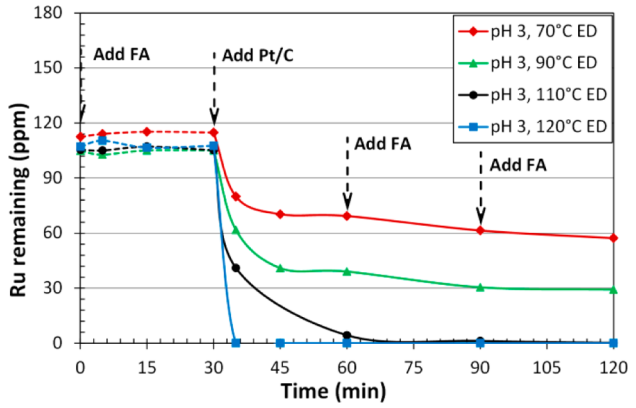

Figure 1. Temperature effect of Ru deposition on Pt/XC-72. Deposition conditions maintained at bath pH 3, deposition time of 2 h, total mole ratio of HCOOH to $Ru(NH_3)_6Cl_3$ = 18:1, and initial Ru^{3+} concentration of 110 ppm. Initial concentration of HCOOH corresponded to $[HCOOH]/[Ru^{3+}]$ = 6/1. The two other aliquots of HCOOH added at 60 and 90 min gave a final mole ratio of 18/1.

when additional aliquots of formic acid were added to the bath. However, when the deposition temperature was increased to 110 °C, all the Ru^{3+} was deposited. The deposition rate was also fastest at 120 °C; all of the Ru deposition was completed in less than 5 min. From these experiments, we can conclude that deposition of $Ru(NH_3)_6^{3+}$ onto Pt/XC-72 is highly temperature-dependent and that both the extent and rate of deposition increase with temperature. The reason for only partial deposition at low temperature (70 and 90 °C) is most likely due to the strong adsorption of CO, the oxidation product of reducing agent formic acid, on surface Pt sites. CO poisoning on Pt surface suppresses and limits further deposition of Ru on Pt surface. A recent study by Baldauf[37] for electrochemical methanol oxidation has shown that poisoning by CO on Pt surfaces occurs at pH 2 and ambient temperatures.

The effects of bath pH on deposition of Ru on Pt are shown in Figure 2. The reaction temperature was kept at 90 °C, and all conditions other than pH were the same as in Figure 1.

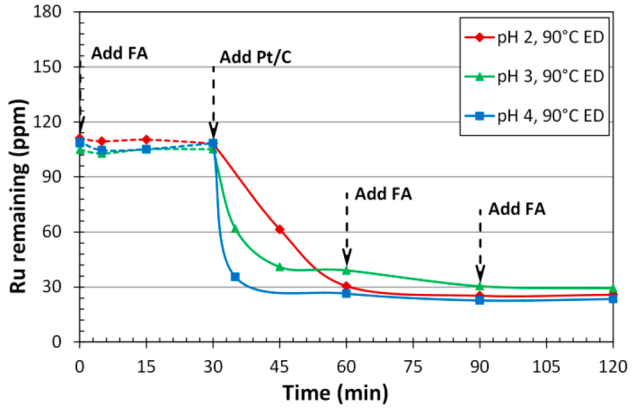

Figure 2. Bath pH effect of Ru deposition on Pt/XC-72. With the exception of a variable pH, the ED conditions were the same as those stated in Figure 1.

The curves in Figure 2 show that the extents of Ru^{3+} deposition were similar for all three pH values, indicating that the pH had little effect on the amount of deposition of $Ru(NH_3)_6^{3+}$ on Pt/XC-72. However, the rates of deposition increased at higher pH values, most likely because the concentration of $HCOO^-$, the active form of the reducing agent, was higher based on the K_a of formic acid at 25 °C (1.8×10^{-4}).

After bath temperature and pH effects were determined, temperatures of 110 °C and pH 3 were chosen to prepare the different weight loadings of Ru on the base 20 wt % Pt/XC-72 catalyst; the results are summarized in Table 1. The amount of Ru deposited was controlled by the initial concentrations of $Ru(NH_3)_6Cl_3$ in the ED bath because ~100% deposition occurred in all cases. This simple relationship of $Ru(NH_3)_6Cl_3$ in the ED bath being proportional to Ru deposition made it straightforward to prepare an extensive series of Ru−Pt bimetallic catalysts, one of the positive features of the ED process. The theoretical coverages of Ru on Pt/XC-72 are shown in the last column of Table 1 and are based on the assumption that Ru is deposited in a monodisperse manner on the Pt surface with a deposition ratio of Ru/Pt = 1:1. Surface compositions are discussed in more detail in Section 3.2.

Table 1. Summary of Pt@Ru/XC-72 Catalysts Prepared by ED[a]

catalysts	Pt wt loading (%)	Ru wt loading (%)	theoretical monodisperse coverage, θ_{Ru}, on Pt	bulk Pt/Ru atomic ratios
Pt@Ru 1	20	0.35	0.16	29.6:1
Pt@Ru 2	20	0.67	0.30	15.5:1
Pt@Ru 3	20	1.03	0.46	10.1:1
Pt@Ru 4	20	1.14	0.51	9.1:1
Pt@Ru 5	20	1.49	0.68	7.0:1
Pt@Ru 6	20	1.83	0.83	5.7:1
Pt@Ru 7	20	2.11	0.96	4.9:1

[a]The compositions are expressed as the weight loadings of Ru deposited on the 20 wt % Pt/XC-72 base catalyst.

3.1.2. Ru@Pt/XC-72 Preparation. To compare with Pt@Ru catalysts, an inverse series of Ru@Pt/XC-72 catalysts were also prepared using electroless deposition. In this case, the base catalyst was 20 wt % Ru/XC-72, also supplied by Premetek. The Ru dispersion was 5.8%, corresponding to an average Ru particle size of 21.1 nm, assuming the H_2 and O_2 adsorption stoichiometries cited earlier. Chloroplatinic acid was used as the Pt source, and DMAB was the reducing agent. To avoid strong electrostatic adsorption of $PtCl_6^{2-}$ on the carbon support, the bath pH was maintained at >9, which was above the PZC of the base 20 wt % Ru/XC-72 catalyst. Each experiment used 0.5 g of the base catalyst in a 100 mL ED bath; the results are summarized in Figure 3. All experiments were conducted for 2 h at 70 °C, and the first 30 min were used to test the thermal stabilities of the ED baths. The Ru/XC-72 catalyst was added to the ED bath at 30 min, and additional DMAB was added at 30 min time intervals.

The deposition curves in Figure 3 show the $PtCl_6^{2-}$ salt was thermally stable with respect to reduction in the presence of DMAB at pH 10 before the addition of 20 wt % Ru/XC-72. In addition to the bath stability test, an earlier control experiment with only H_2PtCl_6 and Ru/XC-72 in a pH 10 solution (without reducing agent) was also conducted under ED conditions. The results showed no $PtCl_6^{2-}$ uptake, which demonstrated that no strong electrostatic adsorption occurred. Thus, on the basis of the control experiment and the bath stability test, we confirm that Pt should be deposited only on the Ru surface and not

DOI: 10.1021/acscatal.5b01011
ACS Catal. 2015, 5, 5123−5134

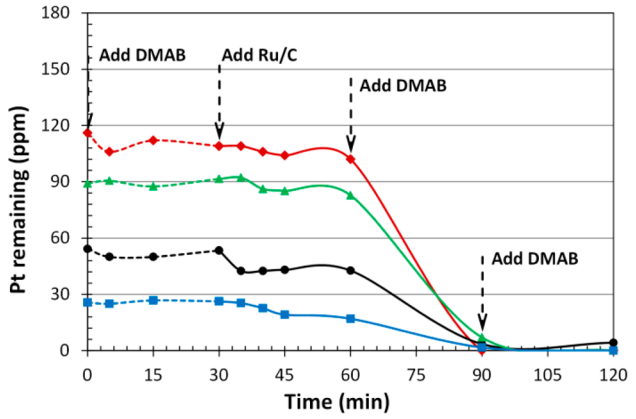

Figure 3. Pt deposition on Ru/XC-72 with different initial concentrations of $PtCl_6^{2-}$. Initial ratio of [DMAB]/[$PtCl_6^{2-}$] = 6/1. Similar amounts of DMAB added at 60 and 90 min to give total ratio of [DMAB]/[$PtCl_6^{2-}$] = 18/1 during the ED experiment.

adsorbed onto the carbon support or reduced in solution. However, when Ru/XC-72 was added at t = 30 min, only negligible amount levels of Pt were deposited between 30 and 60 min, almost certainly because all DMAB added to the bath had been thermally decomposed to produce gas phase H_2 between 0 and 30 min at basic pH values.[38] At 60 min, a second aliquot of DMAB was added to the solution in the presence of Ru/XC-72, this time resulting in facile deposition of Pt on the Ru surface in ≤30 min.

In Figure 3, the concentration of 110 ppm Pt, or 564 umoles $PtCl_6^{2-}$/L, corresponds to one monodisperse layer coverage of Pt on the Ru surface, assuming a 1/1 ratio of Pt to surface Ru. Different weight loadings of Pt on the Ru surface of Ru/XC-72 catalysts were also synthesized by changing the initial concentrations of $PtCl_6^{2-}$ in the bath because all $PtCl_6^{2-}$ in solution was deposited by ED. Table 2 shows the summary of Ru@Pt/XC-72 catalysts prepared by this ED method. As before, the theoretical coverages of Ru on Pt/XC-72 shown in the last column of Table 2 are based on the assumption that Pt is deposited in a monodisperse manner on the Ru surface with a deposition ratio of Pt/Ru = 1:1. All loadings of secondary metal in Tables 1 and 2 were determined from the change of concentration in the ED bath, and not from total digestion of metals from the finished catalyst. On the basis of the phase diagram study by Hutchinson,[39] the bimetallic Pt−Ru compositions in this study (bulk Ru atomic percentages between 0 and 16% and 94.5 and 100%) should remain as core−shell structures, not alloys, at all conditions discussed in this manuscript.

Table 2. Summary of Ru@Pt/XC-72 Catalysts Prepared by ED[a]

catalysts	Ru wt loading (%)	Pt wt loading (%)	theoretical monodisperse coverage, θ_{Pu}, on Ru	bulk Ru/Pt atomic ratios
Ru@Pt 1	20	0.52	0.23	74.2:1
Ru@Pt 2	20	0.99	0.45	39.0:1
Ru@Pt 3	20	1.73	0.79	22.3:1
Ru@Pt 4	20	2.27	1.05	17.0:1

[a]The compositions are expressed as the weight loadings of Pt deposited on the 20 wt % Ru/XC-72 base catalyst.

3.2. Catalyst Characterization. *3.2.1. Chemisorption.* The concentrations of Pt and Ru surface sites for the base Pt/XC-72 and Ru/XC-72 catalysts were determined by pulse chemisorption using hydrogen titration of oxygen-precovered Pt/Ru sites. In general, if adsorbate interactions differ for two metals present on a bimetallic surface, the number of surface sites of each metal can be simply determined. For example, because group IB metals (Cu, Ag, and Au) do not dissociatively chemisorb H_2 at 40 °C but Pd or Pt does, H_2 chemisorption or H_2 titration of oxygen-precovered Pt or Pd can be used to determine the surface coverage of group IB metals on Pt and Pd surfaces.[23,26,40]

Previous work has shown that oxygen precovered Pt surfaces are readily titrated by pulses of 10% H_2/Ar at 40 °C. However, titration of O−Ru sites requires higher temperatures.[31,41,42] The pulse chemisorption results in Figure 4 confirmed this; no measurable titration of O-covered Ru occurred at 40 °C. The situation is much different for O-precovered Pt; for the first five pulses, H_2 was completely consumed, and unreacted H_2 was observed beginning with the sixth pulse and continued until all Pt−O sites were titrated and Pt surface sites were saturated with adsorbed H.

To determine the temperature dependency for reduction of O precovered Ru, temperature-programmed reduction at 10 °C/min (in 10% H_2/balance N_2) over the temperature

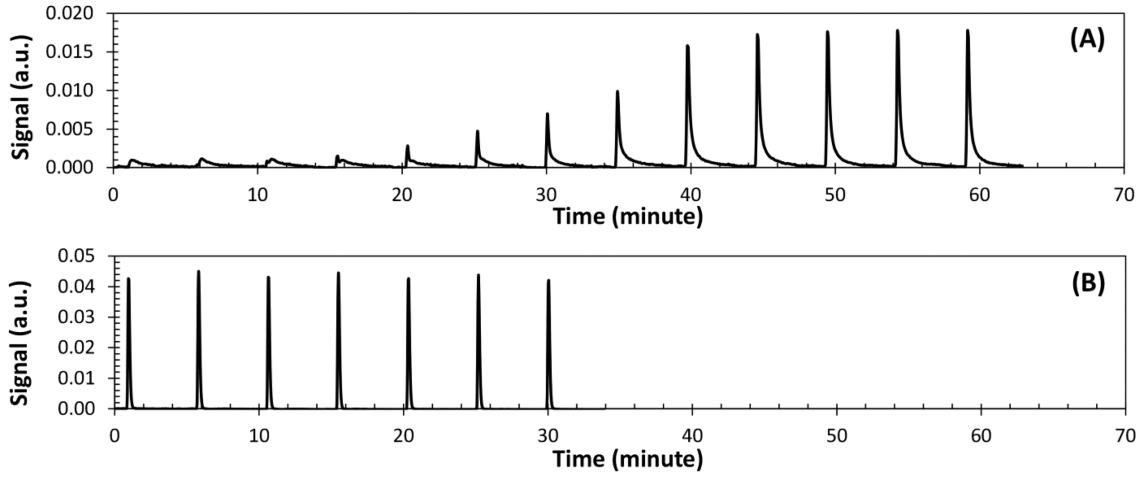

Figure 4. H_2 pulse titrations for O precovered (A) 20 wt % Pt/XC-72 and (B) 20 wt % Ru/XC-72 at 40 °C.

DOI: 10.1021/acscatal.5b01011
ACS Catal. 2015, 5, 5123−5134

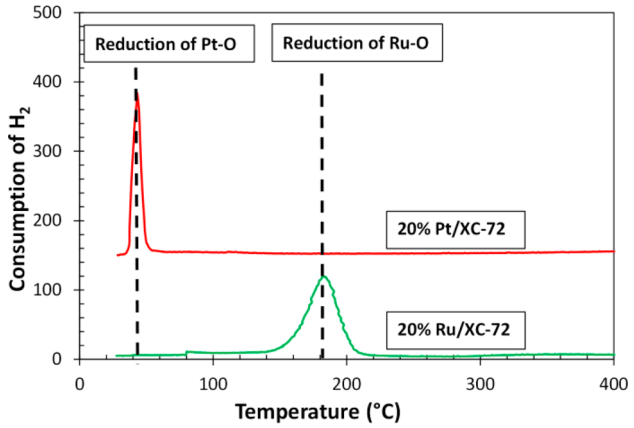

Figure 5. TPR of O-precovered Ru/XC-72 and Pt/XC-72 samples. Temperature ramp rate was 10 °C/min, and sweep gas was N_2.

range 40−400 °C was conducted. The results are shown in Figure 5 and indicate that H_2 titration does not begin until a temperature >150 °C is reached. For comparison, a similar experiment for 20 wt % Pt/XC-72 is also shown and indicates that H_2 titration occurs rapidly at 40 °C. To ensure complete and facile titration of O-precovered Ru, H_2 titration at 250 °C was selected; the pulse chemisorption data are shown in Figure 6. Interestingly, even for the first 10 pulses of H_2, only a constant-valued and partial consumption of H_2 occurred, indicating that the kinetics of Ru−O titration was a slow process, even at 250 °C. The contact time of the H_2 pulse over the Ru−O surface permitted only a limited amount of reaction of H_2 with Ru−O titration to occur. A blank chemisorption experiment for the XC-72 support under the same pretreatment conditions gave no H_2 uptake, indicating that all H_2 uptake values were due to the metallic components.

From H_2 uptake values, the concentrations of Pt and Ru surface sites were calculated to be 1.33×10^{20} and 6.86×10^{19}/g catalyst, respectively, corresponding to 21.5% Pt dispersion and 5.8% Ru dispersion. For the bimetallic catalysts, if there are no chemisorptive interactions between adjacent Pt and Ru sites, H_2 titrations at 40 and 250 °C should separately determine the surface concentrations of Pt and Ru surface sites, respectively. However, H_2 titration experiments for bimetallic Pt@Ru/XC-72 and Ru@Pt/XC-72 catalysts at both 40 and 250 °C always gave H_2 uptake at 40 °C (Pt sites) higher than expected, in fact, even higher than the total number of Pt atoms deposited on the Ru surface for Ru@Pt/XC-72 catalysts. Conversely, H_2 uptakes at 250 °C (Ru sites) were always lower than expected.

3.2.2. Temperature-Programmed Reduction. To better understand the H_2 titration results, temperature-programmed reduction (TPR) of O-precovered, bimetallic Ru−Pt catalysts were conducted from 40−400 °C; the results are summarized

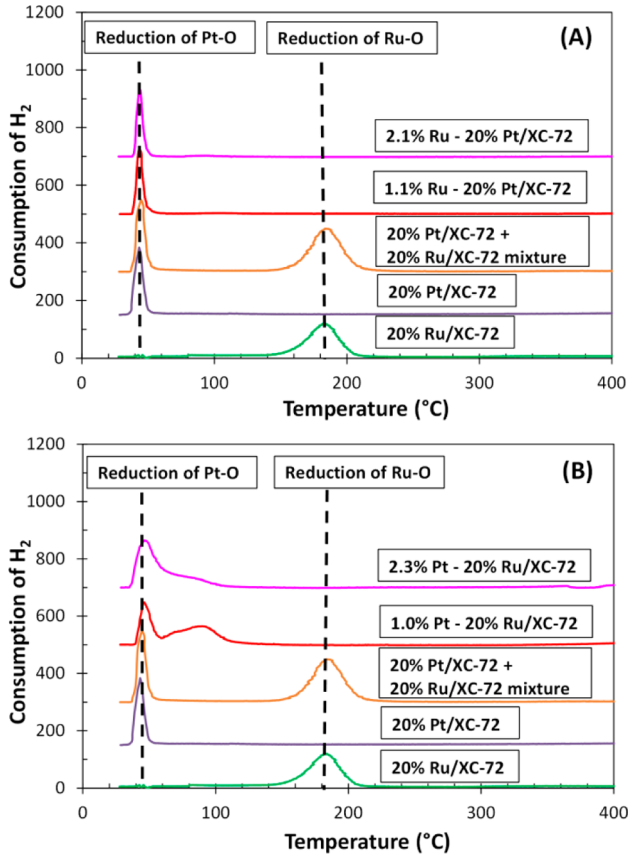

Figure 7. TPR of O-precovered (A) Pt@Ru/XC-72 and (B) Ru@Pt/XC-72 samples. Temperature ramp rate was 10 °C/min, and sweep gas was N_2. TPR curves for 20% Ru/XC-72 and 20% Pt/XC-72 are shown again for reference.

in Figure 7A for ED of Ru on Pt surfaces and in part B for the ED of Pt on Ru surfaces. The TPR curves for monometallic Ru/XC-72 and Pt/XC-72 catalysts are also shown, as well as that for a physical mixture of each of the monometallic catalysts. The results show clearly that reduction of oxygen-precovered Pt/XC-72 occurred sharply at the initial temperature of 40 °C, and reduction of oxygen-precovered Ru/XC-72 was highest at 180 °C. The difference in reduction temperatures confirms that either the surface Ru−O bond is much stronger than the Pt−O bond or dissociative adsorption of H_2 on Ru−O is a thermally activated process. The TPR profile of a physical mixture of Ru/XC-72 and Pt/XC-72 shows both the Pt reduction and Ru reduction peaks, indicating no physical interaction between the Pt and Ru particles.

TPR experiments for Pt@Ru/XC-72 bimetallic catalysts are also shown in Figure 7A. For both 1.1% Ru−20% Pt/XC-72 (theoretical θ_{Ru} = 0.51) and 2.1% Ru−20% Pt/XC-72

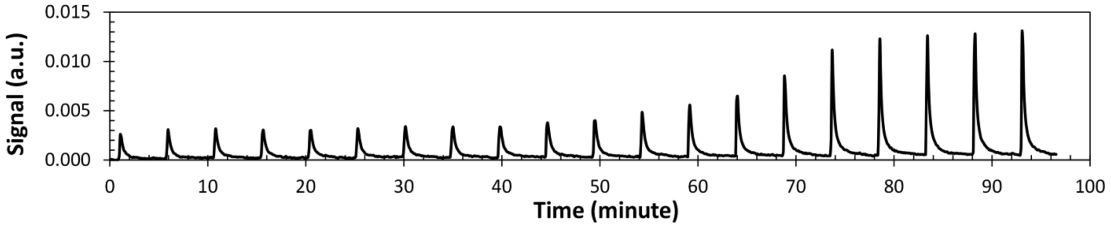

Figure 6. H_2 pulse spectrum for titration of O-precovered Ru/XC-72 at 250 °C.

DOI: 10.1021/acscatal.5b01011
ACS Catal. 2015, 5, 5123−5134

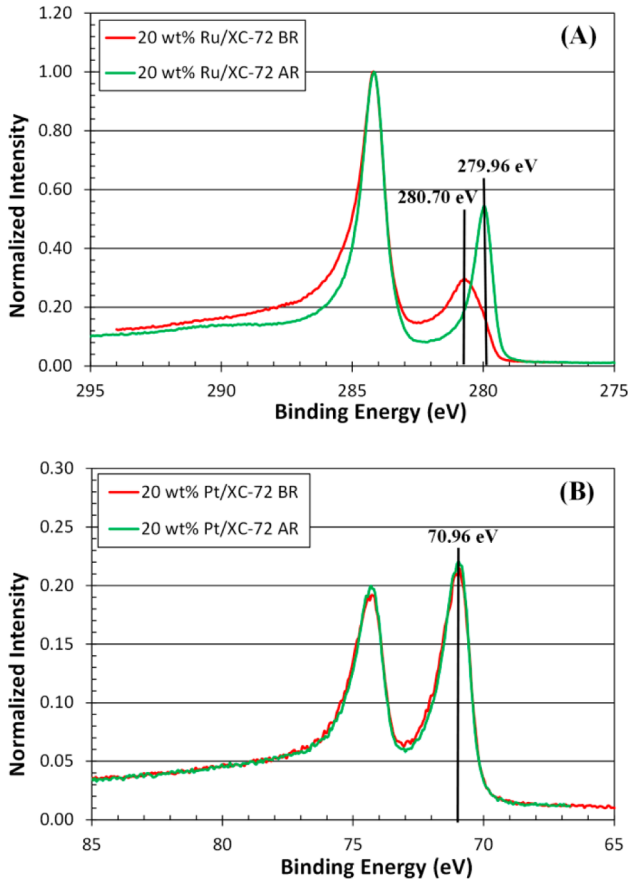

Figure 8. XPS of base catalysts BR and AR at 280 °C for (A) Ru $3d_{5/2}$ and (B) Pt $4f_{7/2}$. The carbon 1s BE at 284.2 eV is also shown in panel A.

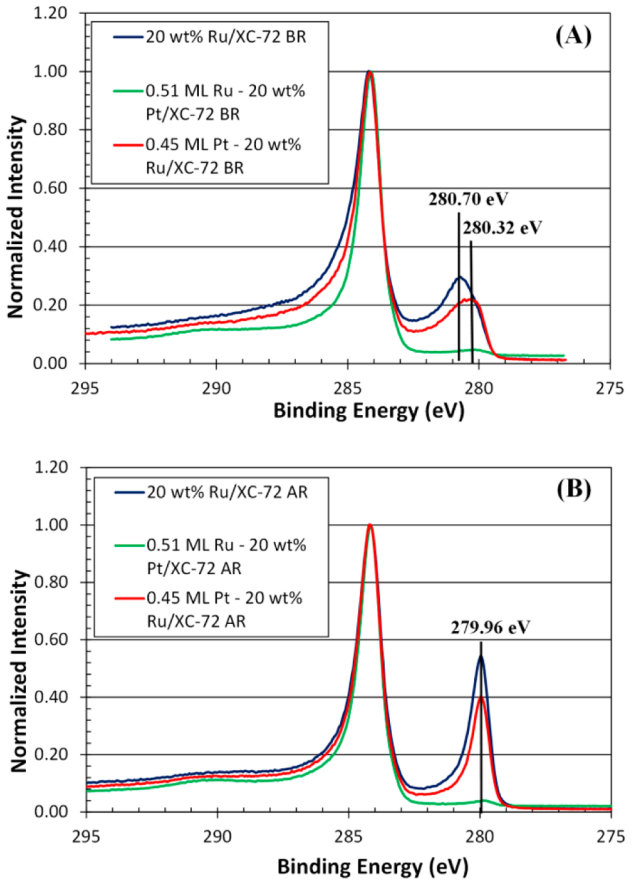

Figure 9. Ru $3d_{5/2}$ peaks of Ru/C, Pt@Ru/C, and Ru@Pt/C (A) before and (B) after 280 °C reduction.

(theoretical θ_{Ru} = 0.96), only the low temperature reduction peak indicative of Pt−O was observed; the Ru−O species was also titrated at 40 °C, explaining why during chemisorption studies the quantity of H_2 consumed was larger than expected. It also indicates there is intimate interaction between the surface Ru and Pt sites, since the titration occurred rapidly at 40 °C. For both Pt@Ru compositions, Ru is the minority component, and there are accessible Pt atoms adjacent to surface Ru atoms. Thus, after titration of the Pt−O site, H_2 can be readily dissociated on the Pt sites to facilitate reduction of adjacent Ru−O at the same temperature. Because there was no TPR peak at 180 °C, the Ru atoms must have been rather evenly distributed on the Pt surface and not in aggregates of isolated Ru−O ensembles on the carbon support. These results also indicate that Ru−O species can be reduced at 40 °C if adsorbed H (from Pt) is present and that the temperature-demanding step for reduction of Ru−O is dissociative adsorption of H_2 on Ru.

TPR profiles of the Ru@Pt/XC-72 catalysts are shown in Figure 7B. The first three TPR curves from the bottom are the same as for panel A. The TPR curve for 1.0% Pt−20% Ru/XC-72 (theoretical θ_{Pt} = 0.45) shows the reduction of Ru−O has been shifted from 180 °C to a broad peak between 60 and 100 °C. Similarly, for 2.3% Pt−20% Ru/XC-72 (theoretical θ_{Pt} = 1.05) the Ru−O reduction peak was shifted to even lower temperatures, existing both as a shoulder of the broader Pt−O reduction peak and as a component of the Pt−O peak at 40 °C. The presence of Pt lowers the reduction temperature to <100 °C again as a result of Pt-assisted reduction of Ru−O. However, because Pt is now the minority component, there are insufficient Pt sites to assist in reduction of all Ru−O species at 40 °C. In addition to insufficient Pt sites adjacent to Ru−O sites, the relatively slow kinetics of H spillover from Pt to Ru may be an additional reason for the reduction peak shoulder between 40 and 100 °C. The broadness of the reduction peak between 40 and 100 °C also indicates that, once formed, Ru^0 sites also participate in the reduction of adjacent Ru−O sites. Combining these two series of TPR experiments with chemisorption measurements, it confirms that the secondary metal (Ru or Pt) was deposited only on the primary metal (Pt or Ru) during ED process and that there are proximal, bimetallic interactions between the two metals.

3.2.3. X-ray Photoelectron Spectroscopy. XPS was used to determine possible electronic interactions between Ru and Pt to investigate the nature of the bimetallic interaction. The BR and AR data for Ru $3d_{5/2}$ and Pt $4f_{7/2}$ binding energies of 20 wt % Ru/XC-72 and 20 wt % Pt/XC-72 are shown in Figure 8. The BE positions and heights of all peaks have been referenced to the C 1s peak of the carbon support for all comparisons. The C 1s peak positions for all samples were constant at 284.2 eV, which is very close to the standard BE of 284.5 eV for conductive carbon surfaces.[43] For the before-reduction sample, the BE for Ru $3d_{5/2}$ corresponds to Ru^{2+} or Ru^{4+} (280.70 eV), revealing the presence of RuO_x on the surface. After reduction at 280 °C, the BE = 279.96 eV indicates complete reduction to Ru^0 (280.0 eV). The Pt $4f_{7/2}$ peak is at 70.96 eV for both before and after reduction at 280 °C, indicating metallic Pt in both

DOI: 10.1021/acscatal.5b01011
ACS Catal. 2015, 5, 5123−5134

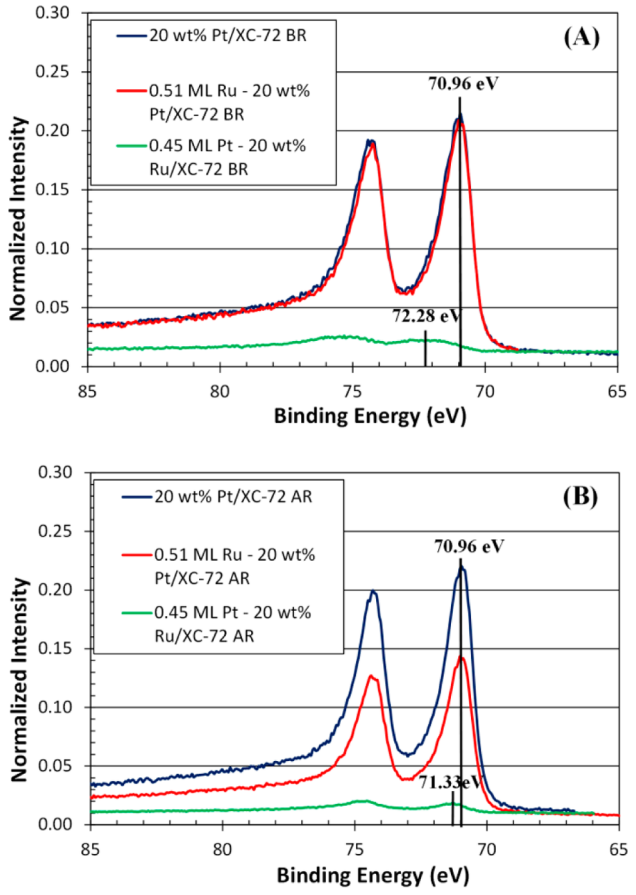

Figure 10. Pt $4f_{7/2}$ peaks for Pt/C, Pt@Ru/C, and Ru@Pt/C (A) before and (B) after 280 °C reduction.

Table 3. Summary of Binding Energies for Ru $3d_{5/2}$ and Pt $4f_{7/2}$

sample	Ru $3d_{5/2}$ before reduction (eV)	Ru $3d_{5/2}$ after reduction (eV)	Pt $4f_{7/2}$ before reduction (eV)	Pt $4f_{7/2}$ after reduction (eV)
20 wt % Pt	N/A	N/A	70.96	70.96
20 wt % Ru	280.70	279.96	N/A	N/A
0.51 ML Ru–20 wt % Pt	280.04	279.87	70.92	70.96
0.45 ML Pt–20 wt % Ru	280.32	279.95	72.28	71.33

cases. Thus, the 20 wt % Pt/XC-72 base catalyst is completely reduced and stable as received from the vendor, whereas the surface of the 20 wt % Ru/XC-72 catalyst was passivated as RuO_x when received from the vendor.

The Ru $3d_{5/2}$ peaks of 0.51 ML Pt@Ru/C and 0.45 ML Ru@Pt/C for before- and after-reduction analyses are shown in Figure 9, along with analogous data for the monometallic catalysts. For the catalysts before reduction, the Ru $3d_{5/2}$ peaks are shifted to lower BEs (280.70 → 280.32 eV) for both bimetallic catalysts, indicating e^- transfer from surface Pt to surface Ru atoms. After reduction, the Ru $3d_{5/2}$ BE values are similar for both Ru only and Ru–Pt bimetallic catalysts, indicating the existence of only Ru^0. For quantitative comparison, the heights of the normalized Ru^0 $3d_{5/2}$ peaks decrease in the order Ru/C > 0.45 ML Ru@Pt/C > 0.51 ML Pt@Ru/C, in agreement with the expected decrease in the Ru surface/near surface concentrations. The substantial decrease in surface Ru

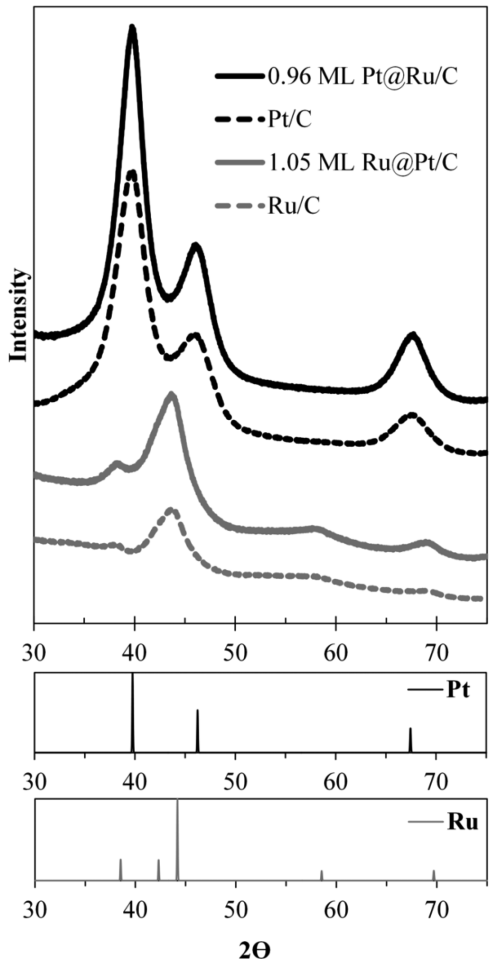

Figure 11. XRD patterns of Pt/C, Ru/C, Pt@Ru/C, and Ru@Pt/C with standard patterns of Pt and Ru phases.

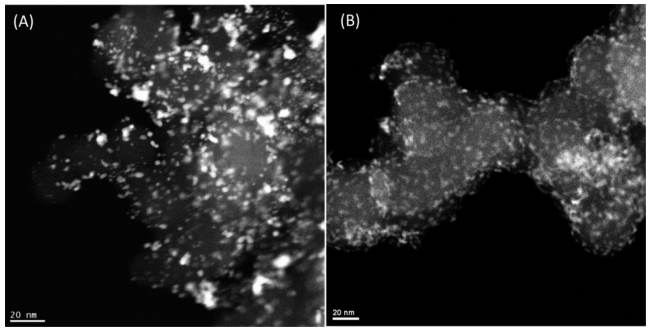

Figure 12. STEM-HAADF micrographs for (A) 20 wt % Pt/C and (B) 20 wt % Ru/C.

for the 0.45 ML Ru@Pt/C (compared with Ru/C) also confirms that Pt atoms have been deposited only on the Ru surface; otherwise, the decrease in the Ru peak intensity would not have been as great.

The Pt $4d_{7/2}$ peaks of Pt/C, 0.51 ML Pt@Ru/C, and 0.45 ML Ru@Pt/C for before- and after-reduction analyses are shown in Figure 10A,B, respectively. For the before-reduction sample of 0.45 ML Ru@Pt/C, the Pt $4d_{7/2}$ peak has shifted to a higher binding energy (70.96 → 72.28 eV), indicating e^- transfer from Pt to Ru atoms, corroborating the results of Figure 9, which showed e^- transfer from Pt to Ru for the

DOI: 10.1021/acscatal.5b01011
ACS Catal. 2015, 5, 5123–5134

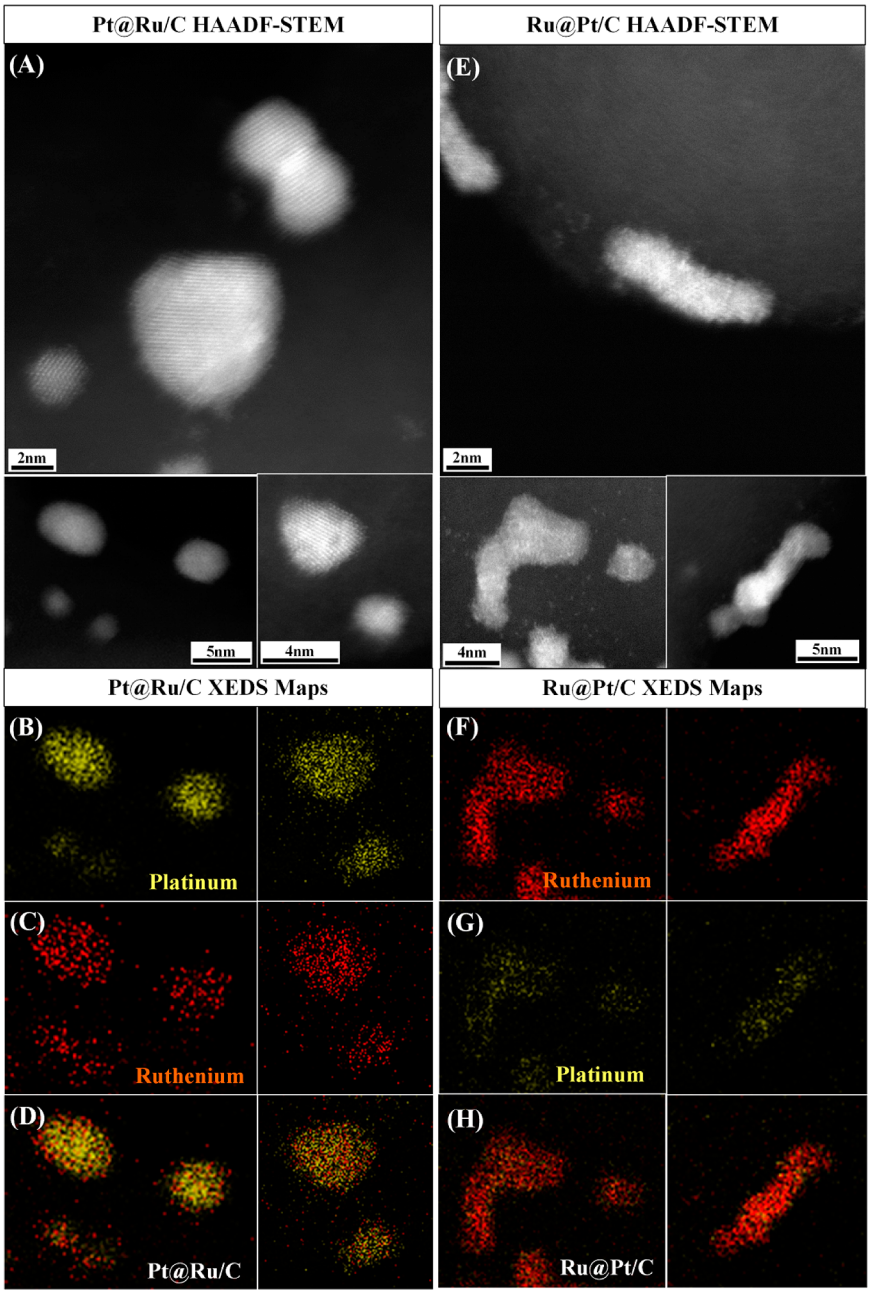

Figure 13. STEM-HAADF micrographs and XEDS maps of (A–D) for Pt@Ru/C and (E–H) for Ru@Pt/C.

0.51 ML Pt@Ru/C sample. In fact, the Pt $4d_{7/2}$ BE value of 72.28 eV is very near the published value of 72.40 eV for Pt^{2+} ($Pt(OH)_2$),[43] indicating a high level of e^- transfer to the oxidized Ru sites. Even after reduction at 280 °C, a BE shift for Pt $4f_{7/2}$ to 71.33 eV is still present, but not as dramatic. The heights of the normalized peaks are in the same order as the decrease in the surface Pt concentration. The XPS results are summarized in Table 3.

In conclusion, XPS analyses confirm that bimetallic interactions exist on the surface of the catalysts, which agrees well with the results from chemisorption and TPR. Further, the directions of the binding energy shifts of both Ru $3d_{5/2}$ and Pt $4d_{7/2}$ peaks demonstrate e^- transfer from Pt to Ru on the bimetallic surface. The shift is more significant for the minority component in the bimetallic system because of the dilution effect of subsurface layers of the majority component.

3.2.4. Powder X-ray Diffraction. Comparison of XRD patterns of the ED-prepared catalysts with the corresponding monometallic base catalysts is shown in Figure 11; the reference patterns of Ru^0 and Pt^0 are also shown. Other than intensity changes, which can be attributed to the amount of sample used during analysis, there are no obvious differences in the patterns for the ED catalysts and their corresponding monometallic base catalysts. There is a slight sharpening of the peaks for both Pt and Ru peaks, which has been attributed to sintering under ED conditions. Schaal[44] observed that sintering of the base metal occurred in some cases as a result of strong interactions between particular reducing agents and metals, such as Pd or Pt.

It is also possible that the apparent increase in size may be due to epitaxial deposition of the secondary metal on the primary metal because the atomic sizes of Ru and Pt are

DOI: 10.1021/acscatal.5b01011
ACS Catal. 2015, 5, 5123–5134

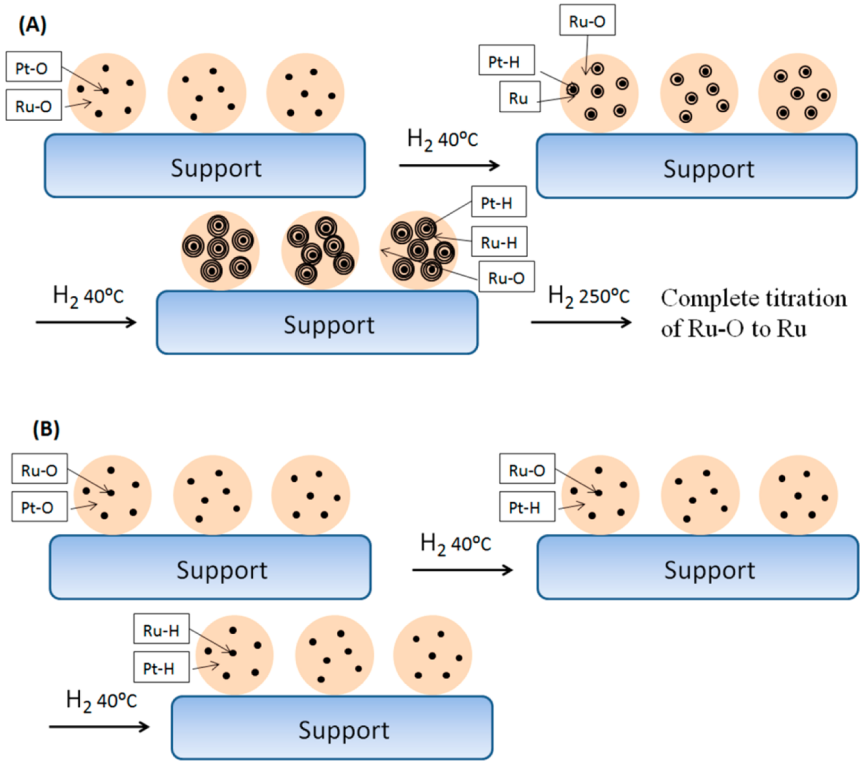

Figure 14. Proposed mechanism for H_2 titration of the O-precovered bimetallic surface of (A) Ru@Pt/C and (B) Pt@Ru/C catalysts.

identical and would not be distinguishable by XRD if lattice parameters of the shell component are the same as the core component. Using the Scherrer equation, the measured peak narrowing corresponds to an ~3 Å increase in particle sizes for both primary metals. Even though there was deposition of the secondary metal from ED bath analysis, failure to observe their XRD peaks can be attributed to the formation of very thin overlayers of the secondary metal, despite the ultralow detection limit of the XRD system. In addition, the peaks observed in the patterns are not shifted relative to the standard positions of the primary metals, indicating that lattice parameters remain the same and there is no alloy formation. These results provide evidence that (1) ED does not favor formation of separate particles of the secondary metal, but that the secondary metal deposits as an overlayer; and (2) the deposited secondary metal overlayer is too thin to be detected by XRD, indicating that the secondary metal is highly dispersed on the primary metal.

3.2.5. Scanning Transmission Electron Microscopy (STEM). Selected HAADF-STEM images of the base catalysts are shown in Figure 12. From these micrographs, the base catalyst particles have significant heterogeneity in size and morphology of the particles. There is considerable clustering of the particles, particularly for the 20 wt % Pt/C catalyst. Irregularities in the size distribution and shape of these particles, however, are not considered influential in the electroless deposition process. Deposition of the secondary metal occurs only on the surface of the accessible primary metal particles, which are measured by chemisorption.

Representative micrographs of the 0.96 ML Pt@Ru/C and 1.05 ML Ru@Pt/C samples are shown in Figure 13A,E. In standard HAADF electron microscopy, also known as Z-contrast imaging, atoms of more massive elements that have a higher Z number produce greater electron scattering. The scattering of electrons is recorded as bright regions in the Z-contrast images. Thus, atoms of heavier elements such as platinum ($Z = 78$) should be brighter than ruthenium ($Z = 44$) in HAADF micrographs, and the carbon support and vacuum are the darkest regions. In the Z-contrast image of the 1.05 ML Ru@Pt/C catalyst (E) the Pt atoms can be made out as faintly brighter regions over a background of less-bright Ru nanoparticles. For the 0.96 ML Pt@Ru/C (A), however, because Ru atoms are deposited over Pt, entire particles show up bright, and thus, regions where Ru is deposited cannot be made out without XEDS mapping of Ru deposition sites.

The XEDS maps of representative spots of the ED catalysts, (B–D) for 0.96 ML Pt@Ru/C and (F–H) for 1.05 ML Ru@Pt/C show more distinct evidence of targeted deposition of the secondary metal on the primary metal. There is correspondence in the location of primary metal, mapped in B and F, to that of the secondary metal, shown in C and G, respectively. This is observed in overlaid maps presented in D and H and was present in virtually all nanoparticles mapped by XEDS. For the 0.96 ML Pt@Ru/C, the Ru map overlaid on the Pt map (D) confirms that Ru is, indeed, present and deposited on the surface of the nanoparticles, which was not clearly observed in HAADF images. Furthermore, the Pt map for the 1.05 ML Ru@Pt/C catalyst (G) corresponds well to the brighter regions of the HAADF image of the same spot (E) which, as discussed earlier, are presumed to be deposited Pt on th basis of Z-contrast. In the XEDS maps, the points of Ru and Pt signals in locations not corresponding to nanoparticles can be attributed to background scattering of spurious X-rays and artifact signal contributions. From these STEM and XEDS images, it is visually established that individual nanoparticles of the catalysts prepared by ED are bimetallic, with excellent association between the primary and secondary metal.

In summary, TPR, XPS, and STEM characterization data have shown that the Pt–Ru catalysts prepared by ED form true

DOI: 10.1021/acscatal.5b01011
ACS Catal. 2015, 5, 5123–5134

bimetallic surfaces with strong interactions between Pt and Ru. Figure 14 shows a model for the surface composition of Pt−Ru bimetals and the resulting mechanism of stepwise reduction that occurs during H_2 titration of the oxygen-precovered Pt−Ru bimetallic system. After pretreatment in flowing O_2, both Pt−O and Ru−O are formed on the bimetallic surface. During dosing with H_2 at 40 °C, the Pt−O surface undergoes reduction to form Pt−H (and H_2O), which can then react with oxygen adsorbed on contiguous Ru−O sites. This Pt-assisted reduction of Ru−O is facile and also occurs at 40 °C to form Ru−H sites, which then assist in reduction of additional and adjacent Ru−O species. For the case of Ru@Pt/C catalysts, in which Ru is the majority component, O chemisorbed on Ru sites not close to Pt will undergo reduction more slowly and will appear as higher-temperature reduction events in the temperature-programmed mode of operation (Figure 7B) and during chemisorption. The continuous outward formation of Ru^0 results in the sequential reduction of the bimetallic surface. For Pt@Ru/C catalysts, in which Ru is the minority component, all O-precovered Ru surface sites are adjacent to surface Pt atoms. The Pt-assisted reduction of Ru−O then occurs completely at 40 °C, as illustrated in Figure 14B. This is also consistent with the TPR data that showed no isolated Ru reduction peak for Pt@Ru/C catalysts.

4. CONCLUSION

Two series of Pt@Ru/C and Ru@Pt/C bimetallic catalysts have been prepared by the electroless deposition method. For Pt@Ru/C preparation, a new ED bath was developed using $Ru(NH_3)_6Cl_3$ as the Ru precursor and HCOOH as the reducing agent. Temperature and pH effects were studied by varying the temperatures from 70 to 120 °C and the pH from 2 to 4. A deposition temperature of 110 °C (to minimize the effects of CO poisoning on the Pt surface during deposition) and a pH of 3 (to avoid strong electrostatic adsorption) were chosen to synthesize Pt@Ru/C catalysts with variable and controlled Ru weight loadings. For Ru@Pt/C preparation, a standard bath using H_2PtCl_6 and DMAB as the Pt precursor and reducing agent, respectively, was employed. Several Ru@Pt/C catalysts with different Pt weight loadings were synthesized by controlling the initial Pt concentrations in the ED bath at the preferred conditions of 70 °C and pH 10.

The Pt@Ru/C and Ru@Pt/C bimetallic catalysts have been characterized by TPR, selective chemisorption, XPS, XRD, and STEM. TPR data showed that for the Ru@Pt/C catalysts, in which Ru was the major component, the peak for the reduction of oxygen-precovered Ru shifted from 180 °C (for monometallic 20 wt % Ru/C) to temperatures between 60 and 100 °C. However, for Pt@Ru/C catalysts, in which Ru was the minor component, the TPR profile resembled that for monometallic 20 wt % Pt/C; both oxygen-covered Pt and Ru surface sites underwent reduction at 40 °C. Selective chemisorption (H_2 titration of oxygen precovered surfaces) experiments also confirmed the existence of strong surface interactions between Pt and Ru, which are explained as hydrogen spillover (Pt-assisted reduction of oxygen precovered Ru). XPS analyses showed that BE shifted to lower values for the Ru $3d_{5/2}$ peak and to higher values for the Pt $4d_{7/2}$ peak. The directions of the binding energy shifts indicate e^- transfer from Pt to Ru on the bimetallic surface, again indicating strong surface interactions between Pt and Ru. There were no obvious differences between the XRD patterns for the ED catalysts and their corresponding base catalysts, revealing that deposition of the second metal by ED bath formed only thin overlayers of the secondary metal, not three-dimensional aggregates. In addition, the peaks observed in the XRD patterns were not shifted relative to the standard positions of the primary metals; the similar lattice parameters remain the same, suggesting no alloy formation. Finally, The STEM and XEDS images provided strong, visual evidence of targeted deposition of the secondary metal on the primary metal. The XEDS images confirmed that individual nanoparticles of the catalysts prepared by ED were bimetallic, with excellent association between the primary and secondary metals. No monometallic Pt or Ru particles were detected for either of the families of bimetallic particles.

AUTHOR INFORMATION

Corresponding Author

*E-mail: monnier@cec.sc.edu.

Notes

The authors declare no competing financial interest.

ACKNOWLEDGMENTS

The authors would like to thank financial support from the University of South Carolina ASPIRE II Grant for Innovative Research. In addition, we gratefully acknowledge Dr. Alan Nicholls from the UIC Research Resources Center for help with STEM/XEDS images and, finally, Yunya Zhang for assistance in manuscript preparation.

REFERENCES

(1) Diaz, G.; Garin, F.; Maire, G. *J. Catal.* **1983**, *82*, 13−25.
(2) Zhang, Y.; Maroto-Valiente, A.; Rodriguez-Ramos, I.; Xin, Q.; Guerrero-Ruiz, A. *Catal. Today* **2004**, *93*−*95*, 619−626.
(3) Diaz, G.; Garin, F.; Maire, G.; Alerasool, S.; Gonzalez, R. D. *Appl. Catal., A* **1995**, *124*, 33−46.
(4) Amano, A.; Parravano, G. *Adv. Catal.* **1957**, *9*, 716−726.
(5) Vu, H.; Goncalves, F.; Philippe, R.; Lamouroux, E.; Corrias, M.; Kihn, Y.; Plee, D.; Kalck, P.; Serp, P. *J. Catal.* **2006**, *240*, 18−22.
(6) Teddy, J.; Falqui, A.; Corrias, A.; Carta, D.; Lecante, P.; Gerber, I.; Serp, P. *J. Catal.* **2011**, *278*, 59−70.
(7) Chatterjee, M.; Zhao, F.; Ikushima, Y. *Adv. Synth. Catal.* **2004**, *346*, 459−466.
(8) Liu, M.; Zhang, J.; Liu, J.; Yu, W. *J. Catal.* **2011**, *278*, 1−7.
(9) Liu, M.; Yu, W.; Liu, H.; Zheng, J. *J. Colloid Interface Sci.* **1999**, *214*, 231−237.
(10) Maris, E. P.; Davis, R. J. *J. Catal.* **2007**, *249*, 328−337.
(11) Claus, P. *Top. Catal.* **1998**, *5*, 51−62.
(12) Gallezot, P.; Richard, D. *Catal. Rev.: Sci. Eng.* **1998**, *40*, 81−126.
(13) Long, J. W.; Stroud, R. M.; Swider-Lyons, K. E.; Rolison, D. R. *J. Phys. Chem. B* **2000**, *104*, 9772−9776.
(14) Hogarth, M. P.; Hards, G. A. *Platinum Met. Rev.* **1996**, *4*, 150−159.
(15) Hamnett, A. *Catal. Today* **1997**, *38*, 445−457.
(16) Wasmus, S.; Kuver, A. *J. Electroanal. Chem.* **1999**, *461*, 14−31.
(17) Garrick, T. R.; Diao, W.; Tengco, J. M.; Monnier, J. R.; Weidner, J. W. *ECS Trans.* **2013**, *53*, 79−84.
(18) Steigerwalt, E. V.; Deluga, G. A.; Lukehart, C. M. *J. Phys. Chem. B* **2002**, *106*, 760−766.
(19) Choi, J.; Park, K.; Kwon, B.; Sung, Y. *J. Electrochem. Soc.* **2003**, *150*, 973−978.
(20) He, Z.; Chen, J.; Liu, D.; Zhou, H.; Kuang, Y. *Diamond Relat. Mater.* **2004**, *13*, 1764−1770.
(21) Coutanceau, C.; Rakotondrainibe, A. F.; Lima, A.; Garnier, E.; Pronier, S.; Leger, J.; Lamy, C. *J. Appl. Electrochem.* **2004**, *34*, 61−66.
(22) Schaal, M. T.; Metcalf, A. Y.; Montoya, J. H.; Wilkinson, J. P.; Stork, C. C.; Williams, C. T.; Monnier, J. R. *Catal. Today* **2007**, *123*, 142−150.

DOI: 10.1021/acscatal.5b01011
ACS Catal. 2015, 5, 5123−5134

(23) Schaal, M. T.; Pickerell, A. C.; Williams, C. T.; Monnier, J. R. *J. Catal.* **2008**, *254*, 131−143.
(24) Beard, K. D.; Borrelli, D.; Cramer, A. M.; Blom, D.; Van Zee, J. W.; Monnier, J. R. *ACS Nano* **2009**, *3*, 2841−2853.
(25) Rebelli, J.; Detwiler, M.; Ma, S.; Williams, C. T.; Monnier, J. R. *J. Catal.* **2010**, *270*, 224−233.
(26) Zhang, Y.; Diao, W.; Williams, C. T.; Monnier, J. R. *Appl. Catal., A* **2014**, *469*, 419−426.
(27) Ohno, I. *Mater. Sci. Eng., A* **1991**, *146*, 33−49.
(28) Galhenage, R. P.; Xie, K.; Diao, W.; Tengco, J. M. M.; Seuser, G. S.; Monnier, J. R.; Chen, D. A. *Phys. Chem. Chem. Phys.* **2015**, DOI: 10.1039/C5CP00075K.
(29) Beard, K. D.; Van Zee, J. W.; Monnier, J. R. *Appl. Catal., B* **2009**, *88*, 185−193.
(30) Ohashi, M.; Beard, K. D.; Ma, S.; Blom, D.; St-Pierre, J.; Van Zee, J. W.; Monnier, J. R. *Electrochim. Acta* **2010**, *55*, 7376−7384.
(31) Liu, D.; Lopez-De Jesus, Y. M.; Monnier, J. R.; Williams, C. T. *J. Catal.* **2010**, *269*, 376−387.
(32) Corro, G.; Gomez, R. *React. Kinet. Catal. Lett.* **1979**, *12*, 145−150.
(33) O'Connell, K.; Regalbuto, J. R. *Catal. Lett.* **2015**, *145*, 777−783.
(34) Regalbuto, J. R. Strong Electrostatic Adsorption of Metals onto Catalyst Supports. In *Catalyst Preparation Science and Engineering*; Regalbuto, J. R., Ed.; CRC Press: Boca Raton, FL, 2007.
(35) Regalbuto, J. R. Electrostatic Adsorption. In *Synthesis of Solid Catalysts*; de Jong, K. P., Ed.; Wiley-VCH Verlag GmbH & Co.: Weinheim, 2009.
(36) Mustain, W. E.; Kim, H.; Narayanan, V.; Osborn, T.; Kohl, P. A. *J. Fuel Cell Sci. Technol.* **2010**, *7*, 041013−041013−7.
(37) Baldauf, M.; Kolb, D. M. *J. Phys. Chem.* **1996**, *100*, 11375−11381.
(38) Djokic, S. S. *Mod. Aspect. Electrochem.* **2002**, *35*, 51−133.
(39) Hutchinson, J. M. *Platinum Met. Rev.* **1972**, *16*, 88−90.
(40) Zhang, Y.; Diao, W.; Monnier, J. R.; Williams, C. T. *Catal. Sci. Technol.* **2015**, *5*, 4123−4132.
(41) Blanchard, G.; Charcosset, H. *Stud. Surf. Sci. Catal.* **1980**, *4*, 515−524.
(42) Kubicka, H. *React. Kinet. Catal. Lett.* **1976**, *5*, 223−228.
(43) Moulder, J. F.; Stickle, W. F.; Sobol, P. E.; Bomben, K. D. In *Handbook of X-ray Photoelectron Spectroscopy*; Physical Electronics Inc.: Eden Prairie, MN, 1995.
(44) Schaal, M. T.; Rebelli, J.; McKerrow, H. M.; Williams, C. T.; Monnier, J. R. *Appl. Catal., A* **2010**, *382*, 49−57.

DOI: 10.1021/acscatal.5b01011
ACS Catal. 2015, 5, 5123−5134